Evaluation of Parallel and Fan-Beam Data Acquisition Geometries and Strategies for Myocardial SPECT Imaging

Yujin Qi, *Member, IEEE*, Benjamin M. W. Tsui, *Senior Member, IEEE*, Karen L. Gilland, *Member, IEEE*, Eric C. Frey, *Member, IEEE*, and Grant T. Gullberg, *Fellow, IEEE*

***Abstract*—This study evaluates myocardial SPECT images obtained from parallel-hole (PH) and fan-beam (FB) collimator geometries using both circular-orbit (CO) and noncircular-orbit (NCO) acquisitions. A newly developed 4-D NURBS-based cardiac-torso (NCAT) phantom was used to simulate the ^{99m}Tc-sestamibi uptakes in human torso with myocardial defects in the left ventricular (LV) wall. Two phantoms were generated to simulate patients with thick and thin body builds. Projection data including the effects of attenuation, collimator-detector response and scatter were generated using SIMSET Monte Carlo simulations. A large number of photon histories were generated such that the projection data were close to noise free. Poisson noise fluctuations were then added to simulate the count densities found in clinical data. Noise-free and noisy projection data were reconstructed using the iterative OS-EM reconstruction algorithm with attenuation compensation. The reconstructed images from noisy projection data show that the noise levels are lower for the FB as compared to the PH collimator due to increase in detected counts. The NCO acquisition method provides slightly better resolution and small improvement in defect contrast as compared to the CO acquisition method in noise-free reconstructed images. Despite lower projection counts the NCO shows the same noise level as the CO in the attenuation corrected reconstruction images. The results from the channelized Hotelling observer (CHO) study show that FB collimator is superior to PH collimator in myocardial defect detection, but the NCO shows no statistical significant difference from the CO for either PH or FB collimator. In conclusion, our results indicate that data acquisition using NCO makes a very small improvement in the resolution over CO for myocardial SPECT imaging. This small improvement does not make a significant difference on myocardial defect detection. However, an FB collimator provides better defect detection than a PH collimator with similar spatial resolution for myocardial SPECT imaging.**

***Index Terms*—Channelized Hotelling observer (CHO), fan beam, ROC analysis, SPECT.**

Manuscript received January 11, 2002; revised February 4, 2004. This work was supported in part by the National Institutes of Health under Grant RO1-HL50663 and by the Director, Office of Science, Office of Biological and Environmental Research, Medical Sciences Division, U.S. Department of Energy under Contract DE-AC03-76SF00098.

Y. J. Qi, B. M. W. Tsui, K. L. Gilland, and E. C. Frey are with the Division of Medical Imaging Physics, Department of Radiology, Johns Hopkins Medical Institutions, Baltimore, MD 21287-0859 USA (e-mail: yqi1@jhmi.edu; btsui1@jhmi.edu; kgillan2@jhmi.edu; efrey@jhmi.edu).

G. T. Gullberg is with the Department of Nuclear Medicine and Functional Imaging, Lawrence Berkeley National Laboratory, Berkeley, CA 94720 USA (e-mail: gtgullberg@lbl.gov).

Digital Object Identifier 10.1109/TNS.2004.829737

I. Introduction

MYOCARDIAL perfusion SPECT images using ^{201}Tl or ^{99m}Tc-sestamibi are an important diagnostic tool in the diagnosis of heart diseases. Over the past several years, a great deal of effort has been made to improve the quality of myocardial SPECT images by developing optimal data acquisition methods [1], [2]. Converging-beam collimators, such as fan and cone beam collimators, have been introduced to improve the tradeoffs between detection efficiency and spatial resolution for cardiac imaging. Data acquisition with a body contour orbit referred to here as noncircular orbit (NCO), which is often used in clinic myocardial SPECT, is expected to have an advantage over a circular orbit (CO) by improving spatial resolution. However, when converging-hole collimators are used, the NCO gives lower detected counts but less truncation as compared to the CO. It is important to know whether there exists an optimal combination of collimator geometry and acquisition orbit for myocardial SPECT imaging. The optimal combination should provide optimal tradeoffs between spatial resolution, contrast and noise in the reconstructed images.

Traditionally, the task-based evaluation of image quality requires human observer studies. However, human observer studies are difficult, time-consuming, and expensive. An alternative using mathematical observer, such as channelized Hotelling observer (CHO), has been proposed and applied to the task-based assessment of image quality [3]–[5]. It has been found that the CHO provided reasonably good predictions of human observer performance even on relatively complex detection tasks involving correlated noise and random backgrounds. In this study we apply the CHO to evaluate combinations of collimator geometries and acquisition strategies for myocardial defect detection. The index of comparisons is the area under the receiver operating characteristics (ROC) curve. We investigate the quality of reconstructed images obtained using different combinations of collimator geometries and data acquisition strategies including CO and NCO. Monte Carlo simulation techniques are used to generate a large number of projection data from a realistic human torso phantom. Image quality indexes such as spatial resolution, contrast and noise were used in the initial evaluation. Evaluation using a CHO study was also performed. Further evaluation using human observers will be used to determine the optimal combination of collimator geometry and orbit for maximum myocardial defect detection.

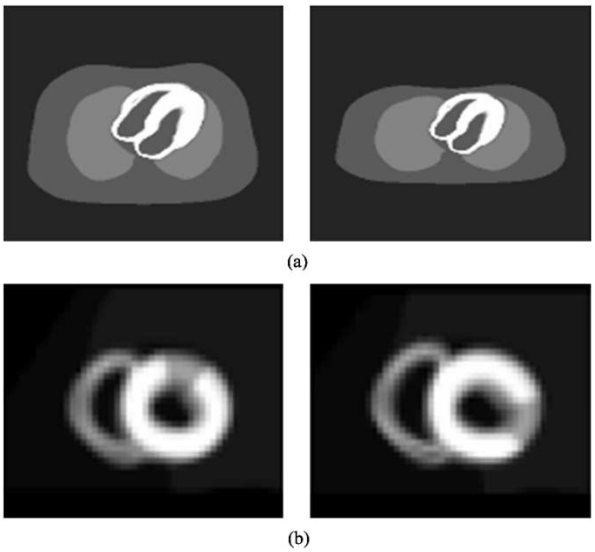

Fig. 1. (a) Sample transaxial image slice through the center of the heart of NCAT phantoms with thick and thin body shapes. (b) Sample of short axis images indicating defects on anterior and lateral walls of the LV. The defect contrast has been enhanced for visualization.

II. Methods

A. Phantoms

The newly developed 4-D NURBS-based cardiac torso (NCAT) phantom [6] was used in this study to simulate patients with different sizes and body shapes. This phantom realistically models the anatomy, attenuation and the activity uptake distribution of ^{99m}Tc-sestamibi in different organs in the upper human torso region. We simulated a typical ^{99m}Tc-sestamibi uptake distribution found in patient studies. The relative activities per unit volume in the torso organs were 37.5, 37.5, 2 and 1 for the myocardium, liver, lung, and body, respectively. The blurring from motion of an average beating heart was included in the phantom.

We generated two phantoms that simulated both thin and thick body shapes of patients, shown in Fig. 1(a), to investigate if a NCO data acquisition method yields improved image quality over that of a CO data acquisition. The thick phantom models a large male patient who has a lateral width of 37 cm and an anterior-posterior (AP) width of 27 cm. The thin phantom modeled thinner patients who have the same lateral width as the thick phantom, but the AP width was reduced to 19 cm. The radius-of-rotation for the CO was set at 22.5 cm while the NCO maintained the body contour with a 1.5" (3.8 cm) gap between the body surface and the camera surface. The ratios of the short axis to the long axis of the noncircular orbits for the thick and thin phantoms were 0.75 and 0.56, respectively.

Two myocardial defects were generated for the NCAT phantom and placed in the following locations: anterior wall midway between base and apex, lateral wall midway between base and anterior wall at the apex, shown in Fig. 1(b). These defects are referred to as the anterior and lateral defects, respectively. All the defects were approximately 60° in circumferential extent and $\sim$2 cm in the longitudinal direction. The radioactivity uptake of the defect was set at 50% lower than the normal myocardium in the defect contrast analysis study. In the CHO study, a 10% defect contrast was used.

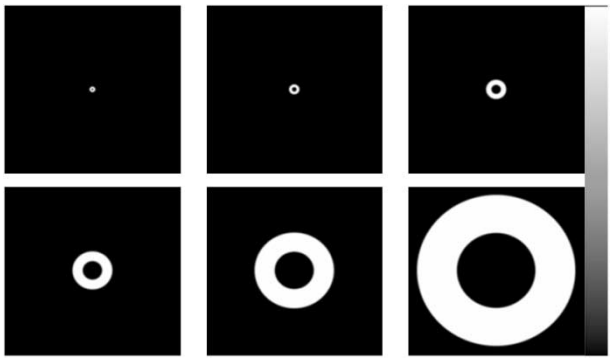

Fig. 2. The frequency channels used in the CHO study.

TABLE I
Relative Detected Counts in Projection Data Using Different Collimator Geometries and Acquisition Orbits

Collimator Geometries	Acquisition Orbits	
	CO	NCO
PH	1.0	1.0
FB	1.52	1.43

TABLE II
The Average Normalized Standard Deviation (NSD) From the Mid-Lateral Region of the Myocardium

	Thick Phantom		Thin Phantom	
	CO	NCO	CO	NCO
PH	0.33	0.33	0.23	0.22
FB	0.26	0.26	0.19	0.18

B. Projection Data Simulations

A modified version of the SIMSET Monte Carlo simulation code [7] was used to generate projection data for both the thick and thin NCAT phantoms using parallel-hole and fan-beam collimators with both CO and NCO data acquisitions. The modifications included adding NCO options into the code, and improving the collimator response for converging collimators, in which the shape of the holes change over the face of the collimators [8]. The projection data included the effects of photon attenuation, collimator-detector response and scatter. The PH and FB collimators were designed to have the same spatial resolution (1.1 cm FWHM) at the center-of-rotation. The collimator hole-length was fixed at 3.5 cm while the hole-size was adjusted around 1.5 mm to give the designed spatial resolution. For the FB collimator the focal length was 65 cm. The field-of-view of the detector was 50×50 cm^2. There was no truncation when the parallel-hole collimator was used and the degree of truncation was small for the FB collimator. There was no truncation of the heart for either collimator. All the projection data were simulated into 128×128 bins and 128 angular views equally spaced over 360°. A large number of photon histories (80 billion) were generated such that the projection data were close to noise-free. Assuming the same total data acquisition time for each collimator and acquisition orbit, the projection data were scaled and Poisson noise fluctuations were added to simulate the count densities found in clinical studies. A total count of 200 K in a 0.312 cm image slice through the center of the heart was used to scale the simulated projection data for the PH collimator.

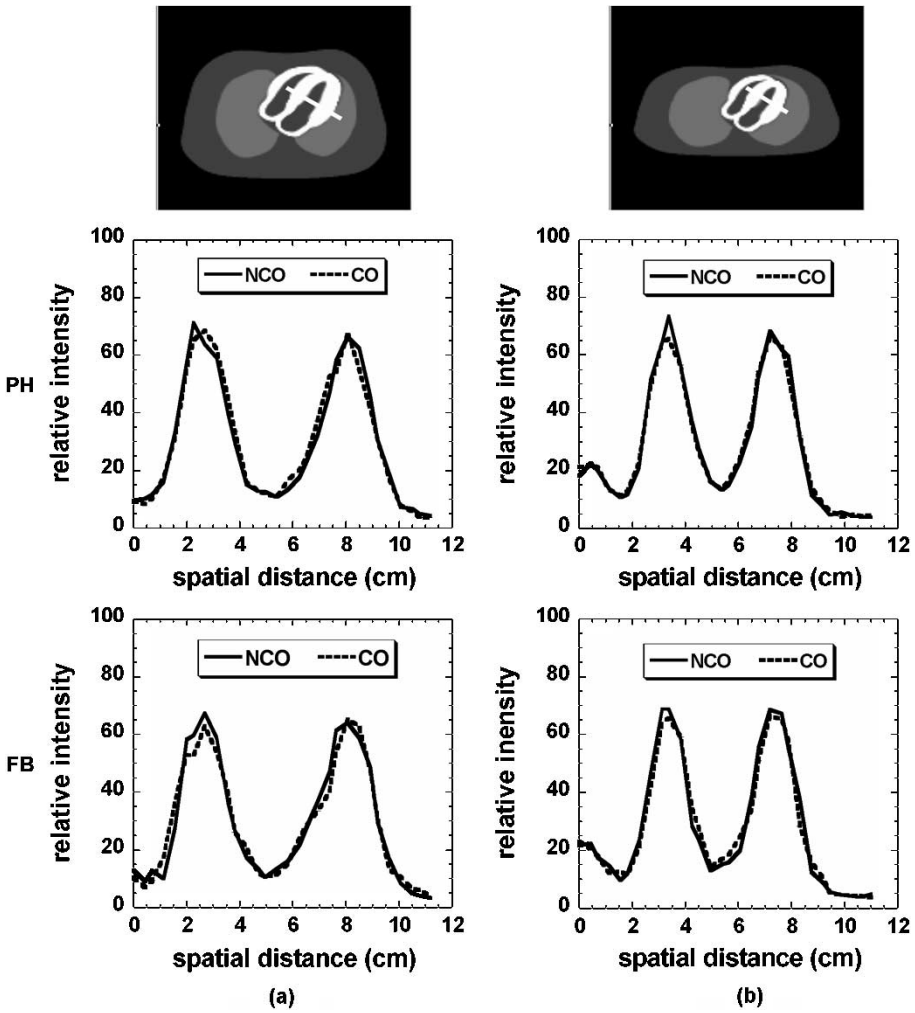

Fig. 3. Profiles through both walls of the LV of a reconstructed transaxial image from the noise-free data. The profile locations were shown in the top row for (a) thick and (b) thin phantoms. The profiles show very small difference in the contrast of the left ventricle wall with respect to the background between CO and NCO for the PH and FB collimator geometries. The profiles show a slightly improvement in spatial resolution for the NCO as compared to the CO for the thin phantom. The images were normalized to the same average count density before taking the profiles.

Then we applied the same scaling factor obtained from the PH collimator to the simulated projection data for the FB collimator since the difference in detection efficiency between the PH and the FB collimators was included in the simulations. All the extensive computing tasks were done on a Linux cluster in the Medical Imaging Research Laboratory, Department of Biomedical Engineering, University of North Carolina at Chapel Hill (UNC-CH). This cluster consists of 18 dual-CPU Pentium III computers.

C. Image Reconstruction and Processing

The noise-free and noisy projection data were reconstructed using the iterative ordered subsets-expectation maximization (OS-EM) reconstruction algorithm with attenuation compensation using 5 iterations and eight angles per subset (16 subsets per iteration). No collimator-detector response and scatter corrections were applied. The attenuation map was blurred using a Gaussian filter with a FWHM of 1.1 cm. All the reconstructed transaxial images were converted to short-axis images for the spatial resolution and CHO analysis.

D. Spatial Resolution and Noise Analysis

In the evaluation study, the effects of the collimator geometry and acquisition strategy on spatial resolution and noise of the reconstructed images were investigated first. The effect of the spatial resolution is related to the defect contrast in the noise-free reconstructed images. The circumferential profiles through the centroid of the lesion were also extracted for comparisons between CO and NCO in the PH and FB collimators for both thick and thin phantoms.

In the analysis of noise, we selected a single transaxial slice through the center of the heart. The noise level was measured using the average normalized standard deviation (NSD) of the pixels in a specified region-of-interest (ROI) within the LV wall. The pixel-by-pixel NSD is defined as the ratio of the estimated standard deviation (s.d.) and mean, i.e.,

$$\mathrm{NSD}_i = \frac{\text{Estimated s.d. at pixel i}}{\text{Ensemble mean value at pixel i}} = \frac{\left[\frac{1}{N-1}\sum_{n=1}^{N}(x_{i,n}-\mu_i)^2\right]^{1/2}}{\mu_i}$$

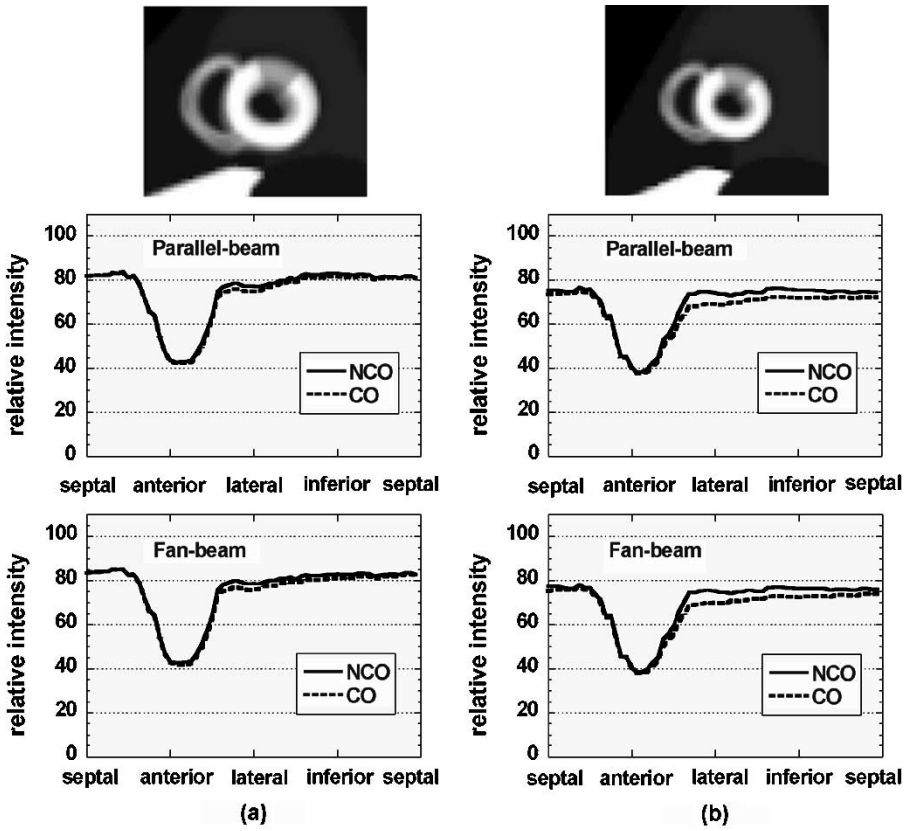

Fig. 4. Comparisons of the circumferential profiles through a short-axis image slice with a myocardial defect in the mid-anterior region for (a) thick and (b) thin phantom. The images were reconstructed from the noise-free projection data and the contrast was 50% with respect to the normal myocardium. The circumferential profiles show larger intensity differences in both lateral and inferior walls between CO and NCO for the thin phantom as compared to the thick phantom.

where $x_{i,n}$ is the value at pixel i for noise realization n, μ_i is the ensemble mean value of pixel i and N is the number of noise realizations. The averaged NSD was obtained from the average of all $\mathrm{NSD_i}$ over all pixels in the lateral wall ROI. For this study, we used 96 noise realizations for each collimator geometry and acquisition orbit.

E. Channelized Hotelling Observer Analysis

For the CHO study, only the thin phantom was used because it provides a bigger difference between the CO and NCO. A single slice of the noisy short-axis images was extracted and then filtered with a 2-D Butterworth filter of order 8 and cutoff frequency of 0.16 cycles/pixel. The single short-axis slice extracted was that containing the defect centroid in the defect-present images. The same slice was extracted on the corresponding defect-absent images. The reconstruction and filter parameter values were chosen based on a previous CHO study with similar images [9].

In the CHO analysis, we used a set of six 2-D, rotationally symmetric frequency channels, with octave-based radial frequency centers and widths and with a square radial profile as shown in Fig. 2. The set of 2-D channels was applied to each of the 2-D noisy short-axis images to produce a collection of six-element feature vectors. The CHOs were then trained and tested using subsets of these feature vectors. We trained the CHO using ensembles of defect-present and defect-absent images. Once the CHO was trained, it was tested by applying it to a different, independent ensemble of feature vectors to produce an ensemble of scaled rating values. These rating values obtained from the testing phase were subsequently analyzed using the ROC methods.

A total of 8 ROC curves were estimated for two lesion locations in the anterior and lateral walls and four acquisition techniques: PH-CO, PH-NCO, FAN-CO and FAN-NCO. For each curve, 48 defect-present and 48 defect-absent short-axis images were used to train the CHO and an additional 48 defect-present and 48 defect-absent short-axis images were used to obtain the rating data. These rating data were then used to estimate ROC curves using the CLABROC code [10]. The area under the ROC curve ($\mathrm{A_Z}$ value) and the standard deviation were also obtained from the code. The $\mathrm{A_Z}$ value was used as the index of comparison. Four combinations of collimator geometries and orbits were compared for each lesion location. These multiple comparisons were tested for statistical significance by adjusting the confidence level to minimize a failure due to random error. For this study, a difference in $\mathrm{A_Z}$ values was deemed statistically significant if the p-value was less than 0.05.

III. Results

A. Spatial Resolution and Noise Analysis Results

From the projection data, we integrated the detected counts over all the 128 views over 360° in a single slice through the center of the heart. The FB collimator with 65 cm focal length provided ~50% increase in detected counts as compared to the PH collimator with similar spatial resolution. Table I shows

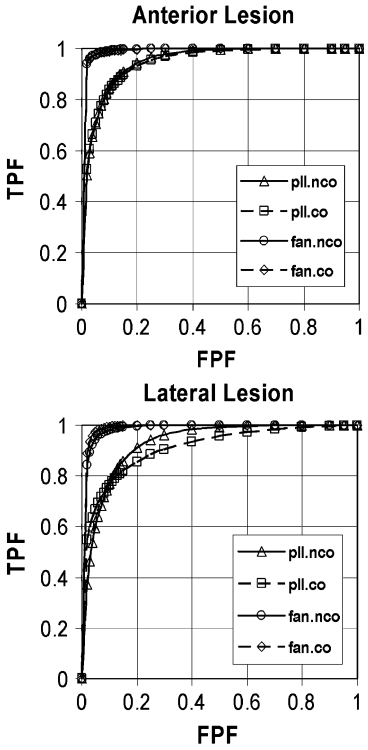

Fig. 5. ROC curves from the CHO study for four combinations of collimator geometries and orbits in detecting the anterior and lateral defects. These curves show that the FB collimator is superior to the PH collimator for a defect detection task.

the relative detected counts in the projection data using different collimator geometries and acquisition orbits for the thin phantom. As expected, the CO offers higher projection counts over the NCO with the FB collimator.

Assuming the same total data acquisition time for each type of collimator, a single transaxial slice through the center of the myocardium was reconstructed with attenuation correction from noisy projection data for both thick and thin phantoms. The relative noise level was determined from the single transaxial slice with 96 realizations. The NSD values obtained from a 32-pixel ROI on the mid-lateral region are shown in Table II. The results show that the NSD values are lower for the FB collimator as compared to the PH collimator, indicating that the noise level is reduced from the PH collimator to the FB collimator as a result of increase in detected counts. Despite the lower detected count density the NCO orbit provides the same noise level as the CO orbit in the attenuation corrected images.

Using the noise-free projection data, we investigated the reconstructed transaxial images in terms of contrast and spatial resolution of the LV walls. Normalized profiles through both of the lateral walls of the LV, are shown in Fig. 3. The profiles show very small differences in the intensity and spatial resolution between CO and NCO for both the PH and FB collimator geometries. The profiles also show a slight improvement in spatial resolution of the LV walls for the NCO as compared to the CO in the thinner phantom.

The myocardial defect contrast was also compared by taking circumferential profiles through the lesion in a short-axis slice obtained with CO and NCO for two different body-shapes using the PH and FB collimators. The circumferential profiles shown in Fig. 4 passed through the anterior defect. The contrast of the defect in the anterior wall shows a small improvement with the NCO acquisition method as compared to the CO acquisition method. The effects are more pronounced in the thinner phantom where the NCO has larger eccentricity.

TABLE III
LISTS OF ESTIMATED A_Z VALUES FOR FOUR ACQUISITION TECHNIQUES WITH DIFFERENT DEFECT LOCATIONS

Acquisition Techniques	A_Z Mean	A_Z St. Dev.	A_Z 95% Confidence Interval
Anterior Lesion			
PH-NCO	0.95	0.02	{0.91, 0.98}
PH-CO	0.95	0.02	{0.91, 0.98}
FB-NCO	0.991	0.004	{0.99, 1.00}
FB-CO	0.995	0.004	{0.99, 1.00}
Lateral Lesion			
PH-NCO	0.93	0.03	{0.89, 0.97}
PH-CO	0.91	0.03	{0.86, 0.96}
FB-NCO	0.99	0.01	{0.97, 1.00}
FB-CO	0.99	0.01	{0.98, 1.00}

TABLE IV
PAIR-WISE COMPARISON OF A_Z VALUES: P-VALUES

Anterior Lesion			
	PH-CO	FB-NCO	FB-CO
PH-NCO	0.9176	0.0329	0.0332
PH-CO		0.0232	0.024
FB-NCO			0.9436
Lateral Lesion			
	PH-CO	FB-NCO	FB-CO
PH-NCO	0.657	0.0347	0.0236
PH-CO		0.0133	0.0082
FB-NCO			0.7467

B. CHO Study Results

Fig. 5 shows the ROC curves obtained from the CHO study for four combinations of collimator geometries and orbits in detecting anterior and lateral defects. The estimated A_Z values and standard deviations from these ROC curves are summarized in Table III. The results show that the FB collimator gives a larger A_Z value than the PH collimator, which indicates that the FB collimator is superior to the PH collimator for myocardial defect detection. In order to study the difference, the statistical pair-wise comparisons of the A_Z were estimated and listed in Table IV. The results show that the differences in A_Z values between FB and PH are statistically significant at $p = 0.05$ level for both the NCO and CO. However, the NCO shows no statistical significant difference from the CO for either the PH or FB collimator.

IV. DISCUSSION

For myocardial SPECT imaging, the data acquisition strategy using a NCO is believed to have an advantage over a CO acquisition by improving spatial resolution. Our results showed very small difference in resolution between the NCO and CO for the

thick and thin phantoms tested in our study. The lesion contrast from the noise-free reconstructed images shows small improvement with the NCO acquisition as compared to the CO acquisition. The effect was more pronounced in the thin phantom as compared to the thick phantom. The CHO analysis also showed no statistically significant difference between NCO and CO for either PH or FB collimator. This result is in agreement with that of a recent clinical study [11].

We also studied the difference in resolution in filtered backprojection reconstructed images obtained using the NCO and CO acquisition methods. The noise-free images from the thin phantom with the PH collimator were used. Again, we found no significant improvement in resolution between NCO and CO acquisition methods.

On the other hand, the improvement of sensitivity by using converging collimator geometry seems to have more effect on defect detection in myocardial SPECT imaging. Our results from the CHO study showed that the defect detectability, which is indexed by an A_Z value, was significantly improved for a FB collimator with 65 cm focal length as compared to a PH collimator with a similar spatial resolution and equal total acquisition time. The improvements A_Z were from 0.95 to 0.99 for an anterior lesion and from $\sim$0.92 to 0.99 for the lateral lesion, respectively. We simulated the projection data at a clinical count level to generate the noisy images for the CHO study. This resulted in fairly high A_Z values. The A_Z values for the FB collimator were very close to 1. The statistical analysis, shown in Table IV, indicated the statistical significance of the comparisons.

V. Conclusion

We have evaluated the detection of myocardial defects in myocardial SPECT images obtained from PH and FB collimator geometries using both CO and NCO acquisition strategies. Results from the spatial resolution and noise analysis indicate that data acquisition using an NCO provides little improvement in resolution and defect contrast over CO acquisition for myocardial SPECT imaging. But this small improvement does not make any significant difference in defect detection from the CHO study. However, the data acquisition geometry using an FB collimator makes a significant improvement in terms of the defect detection as compared to PH collimator with similar spatial resolution and equal total acquisition time.

References

[1] B. M. W. Tsui, J. A. Terry, and G. T. Gullberg, "Evaluation of cardiac cone-beam single photon emission computed tomography using observer performance experiments and receiver operating characteristic analysis," *Invest. Radiol.*, vol. 28, pp. 1101–1112, 1993.

[2] K. J. LaCroix and B. M. W. Tsui, "Investigation of 90° dual-camera half-fan beam collimation for myocardial SPECT imaging," *IEEE Trans. Nucl. Sci.*, vol. 46, pp. 2085–2092, 1999.

[3] W. E. Smith and H. H. Barrett, "Hotelling trace criterion as a figure of merit for the optimization of imaging systems," *J. Opt. Soc. Amer. A*, vol. 4, pp. 717–725, 1986.

[4] K. J. Myers and H. H. Barrett, "Addition of a channel mechanism to the ideal-observer model," *J. Opt. Soc. Amer. A*, vol. 4, pp. 2447–2457, 1987.

[5] H. H. Barrett, J. Yao, J. P. Rolland, and K. J. Myers, "Model observers for assessment of image quality," in *Proc. National Academy of Sciences of the United States of America*, vol. 90, 1993, pp. 9758–9765.

[6] W. P. Segars, "Development of a New Dynamic NURBS-Based Cardiac-Torso (NCAT) Phantom," Ph.D. dissertation, Univ. North Carolina, Chapel Hill, NC, 2001.

[7] R. L. Harrison, S. D. Vannoy, D. R. Haynor, S. B. Gillispie, M. S. Kaplan, and T. K. Lewellen, "Preliminary experience with the photon history generator module of a public-domaon simulation systems for emission tomography," in *IEEE Nuclear Science Symp./Medical Imaging Conf.*, Norfolk, VA, Nov. 1994.

[8] E. C. Frey, B. M. W. Tsui, and G. T. Gullberg, "Improved estimation of detector response function from converging beam collimators," *Phys. Med. Biol.*, vol. 43, pp. 941–950, 1998.

[9] E. C. Frey, K. L. Gilland, and B. M. W. Tsui, "Application of task-based measures of image quality to optimization and evaluation of three-dimensional reconstruction-based compensation methods in myocardial perfusion SPECT," *IEEE Trans. Med. Imaging*, vol. 21, pp. 1040–1050, 2002.

[10] C. E. Metz, P. L. Wang, and H. B. Kronman, "A new approach for testing the significance of differences between ROC curves measured from correlated data," *Inform. Processing Med. Imaging*, pp. 432–445, 1984.

[11] M. P. White, A. Russell, V. A. Mascitelli, R. S. Morris, A. R. Shehata, and G. V. Heller, "Clinical comparison of circular versus noncircular acquisition using technetium-99 m myocardial perfusion SPECT imaging," *J. Nucl. Med. Technol.*, vol. 25, no. 1, pp. 37–40, 1997.